Article

Real-Time Optimization of Organic Rankine Cycle Systems by Extremum-Seeking Control [†]

Andres Hernandez [1,2,*], Adriano Desideri [2], Clara Ionescu [1], Robin De Keyser [1], Vincent Lemort [2] and Sylvain Quoilin [2]

[1]   Department of Electrical Energy, Systems and Automation, Ghent University, 9000 Ghent, Belgium; claramihaela.ionescu@ugent.be (C.I.); robain.dekeyser@ugent.be (R.D.K.)
[2]   Thermodynamics Laboratory, University of Liege, Campus du Sart Tilman B49, 4000 Liege, Belgium; adesideri@ulg.ac.be (A.D.); vincent.lemort@ulg.ac.be (V.L.); squoilin@ulg.ac.be (S.Q.)
[*]   Correspondence: Andres.Hernandez@UGent.be; Tel.:+32-9264-5584
[†]   This paper is an extended version of our paper published in Proceedings of the ASME ORC 2015 Conference, Brussels, Belgium, 12–14 October 2015

Abstract: In this paper, the optimal operation of a stationary sub-critical $11\,kW_{el}$ organic Rankine cycle (ORC) unit for waste heat recovery (WHR) applications is investigated, both in terms of energy production and safety conditions. Simulation results of a validated dynamic model of the ORC power unit are used to derive a correlation for the evaporating temperature, which maximizes the power generation for a range of operating conditions. This idea is further extended using a perturbation-based extremum seeking (ES) algorithm to identify online the optimal evaporating temperature. Regarding safety conditions, we propose the use of the extended prediction self-adaptive control (EPSAC) approach to constrained model predictive control (MPC). Since it uses input/output models for prediction, it avoids the need for state estimators, making it a suitable tool for industrial applications. The performance of the proposed control strategy is compared to PID-like schemes. Results show that EPSAC-MPC is a more effective control strategy, as it allows a safer and more efficient operation of the ORC unit, as it can handle constraints in a natural way, operating close to the boundary conditions where power generation is maximized.

Keywords: extremum-seeking (ES) control; organic Rankine cycle; model predictive control

1. Introduction

In recent years, several studies have underlined the potential of low-grade heat recovery to reduce the amount of worldwide industrial energy consumption [1]. Organic Rankine cycle (ORC) systems are considered a viable and mature technology for waste heat recovery applications in the standard power range (from hundreds of kW_{el} to a few MW_{el}) [2,3]. On the other hand, for micro-WHR applications, the highly fluctuating nature of the heat source makes the development of a reliable ORC unit a challenging task [4,5]. The objectives to optimally operate an ORC power unit for WHR applications can be synthesized in the two following points: (1) keep the cycle in safe working conditions, to preserve the components' life expectancy; (2) maximize the ORC unit net output power, to boost energy production and decrease the payback-time of the installation [6]. In order to achieve these goals, the development of a reliable and effective control strategy able to meet the industrial requirements of simplicity is deemed necessary.

As far as safe working conditions are concerned, a minimum level of superheating must be ensured at the inlet of the expander in order to avoid the formation of liquid droplets that could damage the expansion machine [7,8]. Several contributions focusing on the development of control

strategies to ensure safe working conditions are available in the literature. Traditional control strategies could not offer satisfactory results, as illustrated in [9], where a supervisory predictive control scheme is necessary to achieve the desired performance. Similarly, in [10], the authors implement a predictive functional control and compare its performance to PI controllers, showing that the main challenge for the controller is superheating regulation. Further efforts on better tuning PI-like strategies are reported in [11], where gain-scheduling and feed-forward are implemented to improve PI performance. In [12], an explicit multi-model predictive controller is used to regulate the superheating of an ORC mounted on a heavy duty truck. Multivariable predictive control strategies are also studied as reported in [13,14].

Most of these studies are restricted to guaranteeing safety conditions by regulating the superheating, but little attention has been paid to the performance of the power unit in terms of energy production. In order to maximize the output power, the evaporating temperature is usually considered as the most relevant controlled variable [15,16]. In [17], the modeling and control of a waste heat recovery system for a Euro-VI heavy-duty truck engine was achieved through the use of a switching model predictive control strategy to guarantee the safe operation of the WHR system and to maximize output power. Furthermore, in the automotive field, the problem of maximizing the power produced by an ORC waste heat recovery system on board a diesel-electric rail car is tackled using dynamic real-time optimization [18]. In [16], an experimental study is conducted using an $11\,kW_{el}$ pilot plant, showing that the constrained model predictive control (MPC) outperforms PID-based strategies, as it allows one to accurately regulate the evaporating temperature with a lower control effort while keeping the superheating in a safer operating range.

The latest contributions available in the literature indicate a clear trend towards the preferential use of advanced model-based controllers, especially predictive controllers, over the more traditional PID-based strategy. This is due to their ability to ensure safe and optimal working conditions, especially for WHR applications characterized by highly transient heat source profiles.

In this contribution, we propose a two-layer control structure consisting of a perturbation-based extremum seeking (ES) algorithm coupled to a constrained MPC to guarantee safe and optimal working operation for a stationary sub-critical $11\,kW_{el}$ ORC unit for a WHR application.

Extremum seeking is a well-developed research area that addresses the problem of objective value optimization when the objective function, its gradient and optimum value are unknown [19]. To the best of our knowledge, work has been proposed to optimize vapor compression cycles [20–22] using ES schemes, but this has never been applied to ORC systems. A possible drawback for ES algorithms appears when the extremum causes other variables to violate safety limits. One option to tackle this situation is to design a complex ES algorithm that accounts for constraints, as proposed in [23]. In the present work, we propose to use a simple ES algorithm and let a lower level controller deal with the constraints, e.g., taking actions where the superheating is below a threshold value.

The extended prediction self-adaptive control (EPSAC) approach to constrained model predictive control is proposed as the lower level control strategy. Since it uses input/output models for prediction and not state-space models, as in other MPC algorithms [24], it avoids the need for state estimators, making it a suitable tool for industrial applications. More traditional PI-like strategies are developed for the sake of comparison with the proposed EPSAC-MPC strategy, including a PI controller to regulate superheating at a constant operating point, as is very often done in industrial practice. The control strategies are implemented in MATLAB and tested at the simulation level on a validated nonlinear dynamic model developed in the Modelica language [25]. The coupling between the two software is achieved through the Functional Mockup Interface (FMI) standard. Furthermore, in order to assess the capabilities of the ES algorithm to identify the optimal evaporating condition, the ES algorithm results are compared to the optimal evaporating temperature profile obtained off-line through the nonlinear dynamic model of the ORC unit.

The paper is structured as follows: a description of the $11\,kW_{el}$ sub-critical ORC power system and of the unit Modelica model is presented in Section 2, followed by a description of the adaptive extremum seeking algorithm in Section 3. In Section 4, the EPSAC-MPC algorithm is formulated.

Section 5 is dedicated to the main simulation results and Section 6 to providing some guidelines to tune the extremum seeking algorithm. Finally, a conclusion section summaries the main outcome of this contribution.

2. Process Description

This section describes the architecture and main characteristics of the ORC system used for evaluating the performance of the developed control strategies.

2.1. The Organic Rankine Cycle System

The ORC power unit investigated in this work is a sub-critical $11\,kW_{el}$ experimental unit for stationary low temperature waste heat recovery. The rig is installed at Ghent University campus Kortrijk. The system is based on a regenerative cycle and employs Solkatherm (SES36) as the working fluid. The expander is originally a single-screw compressor adapted to run in expander mode. It drives an asynchronous generator connected to the electric grid through a four-quadrant inverter, which allows varying the generator rotational speed (N_{exp}). The circulating pump is a vertical variable-speed 14-stage centrifugal pump with a maximum pressure of 14 bar and $2.2\,kW_{el}$ nominal power.

Three identical brazed plate heat exchangers are used for the evaporator, internal heat exchanger and condenser. The evaporator is insulated with a glass wool layer of a 180-mm thickness. The Coriolis flow meter enables a direct measurement of the working fluid mass flow rate. Absolute pressure sensors with a range of 0–16 bar are used in conjunction with built-in 4–20-mA transmitters to measure the pressures.

The low-capacity waste heat thermal energy source is ensured by means of an electrical boiler where thermal oil, Therminol66, is pumped through to temperatures of up to 125 °C. The boiler has a maximum power of $250\,kW_{th}$. A PI (proportional integral) controller is implemented to maintain a constant oil temperature at the inlet of the evaporator during transients (e.g., change of ORC pump rotational speed).

A variable flow rate of glycol water (32% ethylene glycol of total volume) is used to cool down the working fluid in the condenser. The thermal energy is rejected by the cooling fluid to the ambient environment by means of an air cooler. A by-pass of the air cooler allows controlling the condenser cooling fluid inlet temperature by means of an adjustable solenoid valve.
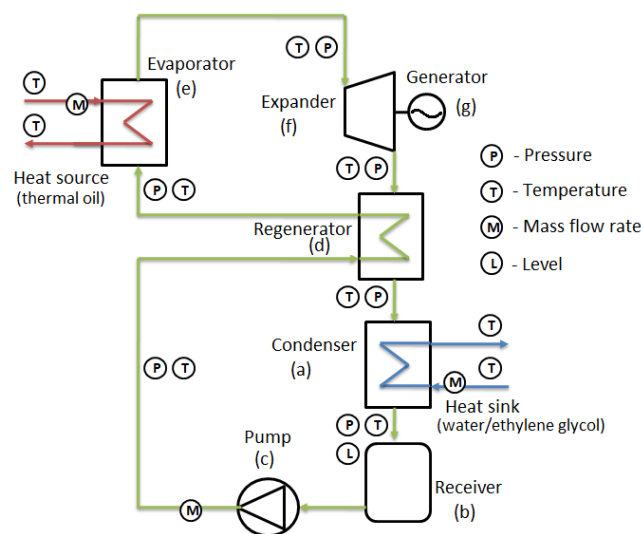

Figure 1. Schematic layout of the pilot plant available at Ghent University, campus Kortrijk (Belgium).

Starting from the bottom of the scheme (Figure 1), it is possible to recognize the liquid receiver (b) installed at the outlet of the condenser (a) where the fluid is collected in saturated liquid condition.

From the receiver outlet, the fluid is pumped (c) through the re-generator (d) cold side and the evaporator (e), where it is heated up to superheated vapor, reaching its maximum temperature at the evaporator outlet. The fluid, after being expanded in the volumetric machine (f), enters the re-generator hot side, and then, it flows into the condenser (a) to close the cycle. The interested reader can refer to [26] for a more detailed description of the ORC test-rig.

2.2. The ORC Unit Modelica Model

In order to assess the performance of the different developed control strategies, a dynamic model of the ORC system presented in Figure 1 has been developed in the Modelica language using existent components from the ThermoCycle library [27]. Dymola is selected as the simulation environment software. The finite volume (FV) modeling approach is used to simulate the three heat exchanger components of the unit. The FV method consists of discretizing the heat exchanger (HE) volume in a number of equal and constant control volumes. It is considered a reliable and robust approach for the modeling of HE involving two-phase fluid flows [25,28].

As the time constants characterizing the compression and expansion processes are negligible compared to the ones characterizing the mass and heat transfer phenomena in the heat exchangers, the pump and the expander are described with semi-empirical quasi-steady-state models. A description of these models is reported in [29]. The liquid receiver at the condenser outlet is modeled assuming thermodynamic equilibrium at all times. Pressure drops in the heat exchangers are lumped at the lowest vapor density section of the ORC system and are modeled according to a quadratic law accounting for linear and turbulent effects [15].

The thermo-physical properties of the working fluid (SES36), the cooling fluid (glycol-water) and the thermal oil (therminol66) are computed coupling Modelica with the open-source fluid properties' library CoolProp [30] through the use of the ExternalMedia package [27]. For a more detailed description of the modeling approach, the interested reader can refer to [25].

The developed Modelica model is then exported into the Simulink/MATLAB environment by means of the Functional Mockup Interface (FMI) open standard, using a model exchange format. This simulation approach takes advantage of the strengths of each platform: Modelica for modeling and Simulink/MATLAB for control design. The presented simulation results are performed with an expander rotational speed set constant at 3000 rpm, so as to emulate an installation directly connected to the grid.

2.3. ORC Unit Optimal Working Conditions

In order to optimally operate a sub-critical ORC unit for waste heat recovery applications, two main conditions need to be satisfied: (1) ensure safe working operation; and (2) maximize the net output power.

As far as safety operations are concerned, a super-heated vapor state must be ensured at the expander inlet. In applied thermodynamic terms, an accurate regulation of the superheating (ΔT_{sh}) is deemed fundamental to avoid a wet expansion: the formation of liquid droplets during the expansion process that could damage the machine.

The superheating is defined as:

$$\Delta T_{sh} = T_{exp,su} - T_{sat,ev} \tag{1}$$

where $T_{exp,su}$ is the temperature measured at the inlet of the expander and $T_{sat,ev}$ the evaporating temperature at the evaporating pressure $p_{sat,ev}$.

For waste heat recovery applications in order to optimize the ORC unit performance, the net output power needs to be maximized during operation. In this regard, the evaporating temperature

is considered the most relevant control variable [16]. The net output power is selected as the most relevant performance index and is defined by:

$$\dot{W}_{el,net} = \dot{W}_{exp} - \dot{W}_{pump} \tag{2}$$

The cycle first law efficiency is also provided for indicative purposes and is defined by:

$$\eta_{cycle} = \frac{\dot{W}_{el,net}}{\dot{Q}_{in,ORC}} \tag{3}$$

where $\dot{W}_{exp}$ is the expander electrical power, $\dot{W}_{pump}$ is the pump electrical power and $\dot{Q}_{in,ORC}$ is the thermal power supplied to the ORC working fluid in the evaporator.

2.4. ORC Unit Model-Based Investigation

The developed Modelica dynamic model is used to gain insight into the system's dynamics, in particular the relationship between superheating (ΔT_{sh}), evaporating temperature ($T_{sat,ev}$), pump speed (N_{pp}) and expander electrical power ($\dot{W}_{exp}$).

The system is perturbed by applying 100 rpm step changes on the pump rotational speed in the range between 1300 and 2100 rpm for different heat source conditions. The heat source temperature, T_{hf}, is varied between 90 and 125 °C while the heat source mass flow, $\dot{m}_{hf}$, is comprised of a range between 0.5 and 1.5 kg/s. The heat sink temperature, T_{cf}, and heat sink mass flow, $\dot{m}_{cf}$, were kept constant at 15 °C and 4 kg/s, respectively. The steady-state values obtained at each pump speed are depicted in Figure 2, where the expander electrical power $\dot{W}_{exp}$ is represented as a function of $T_{sat,ev}$ and ΔT_{sh}.
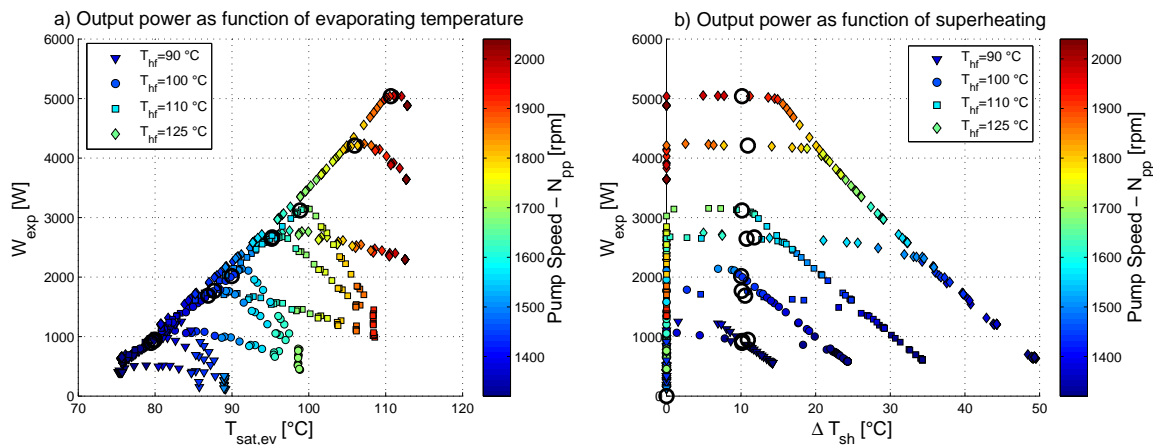

Figure 2. Expander output power *versus* (**a**) evaporating temperature and (**b**) superheating for different heat source conditions $T_{hf} = \{90, 100, 110, 125\}$ °C with $\dot{m}_{hf} = \{0.5, 1.0, 1.5\}$ kg/s.

Figure 2a illustrates that for each heat source condition, there exists an optimal evaporating temperature that maximizes the expander output power: as an example, for a heat source of 1.5 kg/s and 125 °C, an optimum is reached for $T_{sat,ev} = 112$ °C, corresponding to an output power of 5 kW.

As the pump speed is increased, the working fluid mass flow and the superheating decreases, extracting more thermal energy from the heat source and consequently leading to an electrical power increment. In Figure 2b, the influence of the pump speed and the superheating level on the expander output power is reported. Once the superheating reaches zero (*i.e.*, the fluid is in the two-phase condition), the expander power drops.

The model-based investigation allows one to conclude that the ORC unit output power is inversely proportional to the degree of superheating in the evaporator, and it exhibits an optimum as a function of the evaporating temperature. For limited values of the superheating (e.g., lower than 10 °C), the

gain in output power remains limited (about 1.12%), which indicates an acceptable target range for the control.

Based on the acquired simulation data, it is possible to derive a correlation describing the optimal evaporating temperature as a function of the heat source conditions:

$$T_{sat,opt} = -290.915 + 183.33 \cdot log_{10}(T_{hf}) + 10.636 \cdot \dot{m}_{hf} \tag{4}$$

Equation (4) is valid in the range of $0.5 \leq \dot{m}_{hf} \leq 1.5 \, \text{kg/s}$ and $90 \leq T_{hf} \leq 125 \, ^\circ\text{C}$ given a constant saturation temperature in the condenser of $p_{sat,cd} = 1.4 \, \text{bar}$. It is computed considering a minimum superheating value of $10 \, ^\circ\text{C}$, as represented by the black circles in Figure 2 and provides an accuracy of $R^2 = 98.7\%$.

Based on the obtained simulation results, it is concluded that the design of a control strategy focusing on the regulation of the evaporating temperature while ensuring a minimum amount of superheating is deemed necessary for optimal operation. Controlling the expander speed or turbine guide vanes is not considered in the present work, since it constitutes an additional system complexity and cost and is not implemented in most commercial ORC systems [4].

3. Adaptive Optimization

The identification of the optimal evaporating temperature is a fundamental step towards the implementation of a control strategy aimed at maximizing the output power of the sub-critical ORC unit. If a dynamic model of the system is available and calibrated for the target system, an optimal correlation can be developed, which further satisfies the system safety constraints (*cf.* Equation (4)). However, there are two drawbacks in this approach: (1) a validated dynamic model is not always available; (2) model errors can bias the computed optimal operating conditions.

In order to overcome these issues, we propose a different approach based on the implementation of an extremum seeking (ES) algorithm. Such an approach allows identifying the optimal evaporating temperature, without the need for a model of the investigated system. Extremum seeking is a well-developed field that addresses the problem of objective value optimization when the objective function, its gradient and optimum value are unknown [19]. From the different algorithm variations, the perturbation-based ES framework is the most popular method in the literature [19], as it has proven to be more robust to noise and dynamic effects in the system, thus producing smoother references, which decrease the risk of instability [31].

The schematic representation of the proposed control structure is depicted in Figure 3. The perturbation-based ES algorithmis in charge of finding the extremum $T_{sat,opt}$ that arises from the reference-to-output nonlinear map (*i.e.*, $T_{sat,ev}$ to $\dot{W}_{exp}$), while a low-level feedback controller keeps the system stable at that equilibrium optimal point.
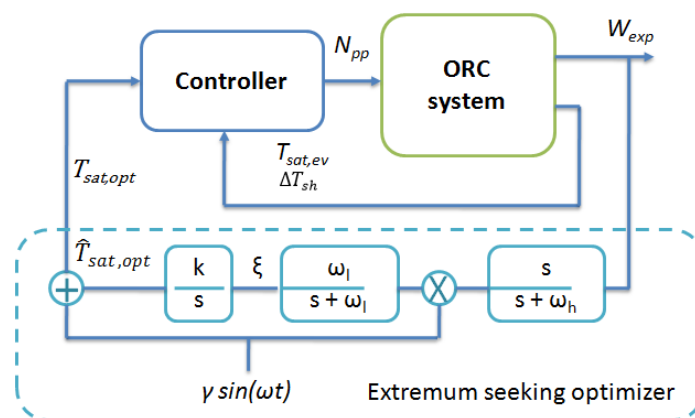

Figure 3. Perturbation-based extremum seeking algorithm applied to the ORC system.

The working principle of the ES algorithm is depicted in Figure 4. The ES algorithm estimates the gradient of the nonlinear mapping, f, by perturbing its input with a periodic dither signal with radial frequency ω and by processing its output $\dot{W}_{exp}$. Although the relationship between $\dot{W}_{exp}$ and $T_{sat,ev}$ is nonlinear and *a priori* unknown, it is assumed that an extremum $\dot{W}_{exp,opt} = f(Tsat, ev)$ exists.

In this study, the dither signal is assumed to be a sine wave, although other types of dither can be used, as well [32]. Figure 4 shows the response of a nonlinear function with a global maximum to such a sinusoidal perturbation signal around three different $\hat{T}_{sat,opt}$. At $\hat{T}_{sat,opt\,1}$, $\frac{\partial f(\hat{T}_{sat,opt\,1})}{\partial T_{sat,opt}} < 0$, resulting in an inversion of the dither signal phase in the output of the nonlinear function. Instead, at $\hat{T}_{sat,opt\,3}$, $\frac{\partial f(\hat{T}_{sat,opt\,3})}{\partial T_{sat,opt}} > 0$, the phase of the dither signal component remains unchanged.
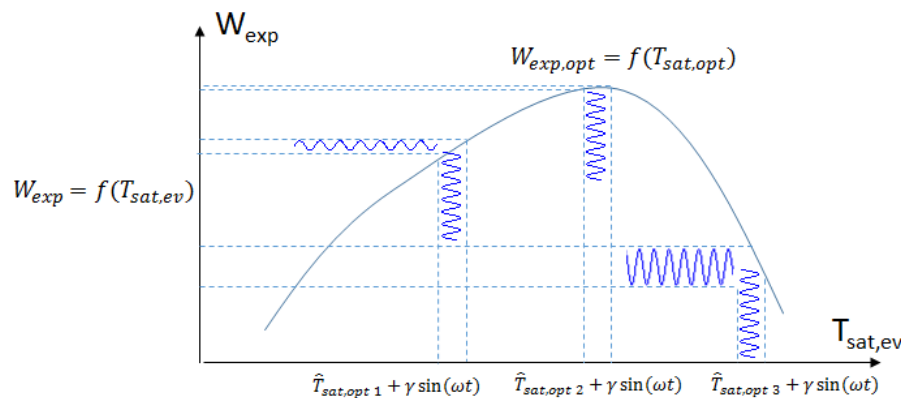

Figure 4. Sinusoidal perturbation around various $\hat{T}_{sat,opt}$.

The perturbation around $\hat{T}_{sat,opt\,3}$ results in a larger amplification of the dither signal, compared to perturbation around $\hat{T}_{sat,opt\,1}$. Around $\hat{T}_{sat,opt\,2}$, which is close to the extremum $T_{sat,opt}$, the dither signal is hardly visible in the output, because $|\frac{\partial f(\hat{T}_{sat,opt\,1})}{\partial T_{sat,opt}}| \approx 0$. Furthermore, in this figure, $|\frac{\partial f(\hat{T}_{sat,opt\,2})}{\partial T_{sat,opt}}| < |\frac{\partial f(\hat{T}_{sat,opt\,1})}{\partial T_{sat,opt}}| < |\frac{\partial f(\hat{T}_{sat,opt\,3})}{\partial T_{sat,opt}}|$. Intuitively, the dither signal component in the output can be regarded as an estimate of the local gradient around a certain $\hat{T}_{sat,opt}$

The reference to the low-level controller consists of the sine wave dither signal and an adaptation input:

$$T_{sat,opt} = \gamma \, sin(\omega t) + \hat{T}_{sat,opt} \tag{5}$$

where γ is the amplitude and ω is the modulation frequency. The adaptation signal, $\hat{T}_{sat,opt}$, shifts the sine wave towards the gradient direction. The response of the system to this signal is measured in the objective value ($\dot{W}_{exp}$). This output is filtered by a high-pass filter to eliminate the DC component and demodulated by the same sine signal to extract the gradient direction. Note that filters and integrator are represented using the Laplace variable s.

$$\xi = \dot{W}_{exp} \left(\frac{\omega_l}{s + \omega_l} \right) \left(\frac{s}{s + \omega_h} \right) (\gamma \, sin(\omega t)) \tag{6}$$

This information is used to calculate the shift in the sine signal towards the gradient. The adaptation law is then computed by:

$$\hat{T}_{sat,opt} = \xi \, \frac{k}{s} \tag{7}$$

where k is a positive constant that specifies the adaptation speed. Since only the DC component of the demodulated signal is needed for gradient calculation, a low pass filter is often used. The amplitude

and frequency of the sine wave signal and the cutoff frequencies of the filters are important design parameters. A detailed study of how the design of the perturbation signal affects the performance of the ES algorithm is presented in [32].

4. Model Predictive Control

A brief introduction to the EPSAC algorithm is presented in this section. For a detailed description, the reader is referred to [16,33].

4.1. Computing the Predictions

Using the EPSAC algorithm, the measured process output $y(t)$ can be represented using Equation (8), as illustrated in Figure 5.

$$y(t) = x(t) + n(t) \tag{8}$$

where $x(t)$ is the model output that represents the effect of the control input $u(t)$ and $n(t)$ represents the effect of the disturbances and modeling errors, all at discrete-time index t.
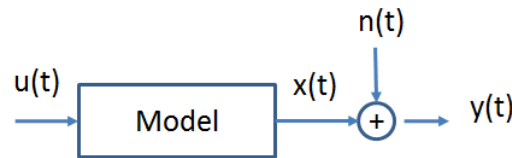

Figure 5. Process model in the EPSAC algorithm.

Model output $x(t)$ can be described by the generic system dynamic model:

$$x(t) = f\left[x(t-1), x(t-2), \ldots, u(t-1), u(t-2), \ldots\right] \tag{9}$$

Notice that $x(t)$ represents here the model output, not the state vector. Also important is the fact that f can be either a linear or a nonlinear function. Furthermore, the disturbance $n(t)$ can be modeled as colored noise through a filter with the transfer function:

$$n(t) = \frac{C(q^{-1})}{D(q^{-1})} e(t) \tag{10}$$

where $e(t)$ is uncorrelated (white) noise with zero-mean and C, D are monic polynomials in the backward shift operator q^{-1}. The disturbance model must be designed to achieve the robustness of the control loop against unmeasured disturbances and modeling errors [24].

Using the generic process model (Equation (8)), the predicted values of the output are represented in Equation (11). Notice the notation $\ldots(t+k|t)$, which denotes the future values up to time $t+k$ of a signal, postulated at time t.

$$y(t+k|t) = x(t+k|t) + n(t+k|t) \tag{11}$$

where $x(t+k|t)$ and $n(t+k|t)$ can be predicted by recursion of the process model (Equation (9)) and by using filtering techniques on the noise model (Equation (10)), respectively [33]. Notice that $u(t+k|t)$ denotes future values of the input, postulated at time t.

4.2. Computing the Optimal Control Action

A key element in linear MPC is the use of base (or free) and optimizing (or forced) response concepts [34]. In EPSAC, the future response can be expressed as:

$$y(t + k|t) = y_{base}(t + k|t) + y_{optimize}(t + k|t) \tag{12}$$

The two contributing factors have the following origin:

- $y_{base}(t + k|t)$ is the effect of the past inputs, the *a priori*-defined future base control sequence $u_{base}(t + k|t)$ and the predicted disturbance $n(t + k|t)$.
- $y_{optimize}(t + k|t)$ is the effect of the additions $\delta u(t + k|t)$ that are optimized and added to $u_{base}(t + k|t)$, according to $\delta u(t + k|t) = u(t + k|t) - u_{base}(t + k|t)$. The effect of these additions is the discrete time convolution of $\Delta U = \{\delta u(t|t), \ldots, \delta u(t + N_u - 1|t)\}$ with the impulse response coefficients of the system (G matrix), where N_u is the chosen control horizon.

The control ΔU is the solution to the following constrained optimization problem:

$$\Delta U = arg \min_{\Delta U \in \mathbb{R}^{N_u}} \sum_{k=N_1}^{N_2} [r(t + k|t) - y(t + k|t)]^2$$

$$s.t. \ A.\Delta U \leq B \tag{13}$$

where N_1 and N_2 are the minimum and maximum prediction horizons, N_u is the control horizon and $r(t + k|t)$ is a future setpoint or reference sequence. The various process input and output constraints can all be expressed in terms of ΔU, resulting in matrices A, B. Since Equation (13) is quadratic with linear constraints in decision variables ΔU, then the minimization problem can be solved by a quadratic programming (QP) algorithm [24,34].

4.3. Low-Order Model for Prediction

In order to obtain the low-order model required by the MPC strategy, a parametric identification procedure is performed. Two models are identified from the manipulated variable: pump speed (N_{pp}) to the evaporating temperature ($T_{sat,ev}$) and superheating (ΔT_{sh}).

Notice that the heat source temperature (T_{hf}) also influences evaporating temperature and superheating, thus becoming a measured disturbance. As a result, we are interested in identifying a system consisting of two inputs (one manipulated (N_{pp}) and one measured disturbance T_{hf}) and two outputs ($T_{sat,ev}$ and ΔT_{sh}). A linear parametric identification is thus performed in the system using the prediction error minimization method from the data collected using a multisine excitation signal [35]. The identified model presented in (Equation (14)) is in the form of discrete-time transfer functions for a sampling time $T_s = 1$ s.

$$\Delta T_{sh}(t) = \frac{-0.063q^{-1} + 0.059q^{-2}}{1 - 2.44q^{-1} + 1.955q^{-2} - 0.51q^{-3}} N_{pp}(t) + \frac{0.47q^{-1}}{1 - 0.51q^{-1}} T_{hf}(t) \tag{14a}$$

$$T_{sat,ev}(t) = \frac{0.066q^{-1} - 0.063q^{-2}}{1 - 2.42q^{-1} + 1.91q^{-2} - 0.49q^{-3}} N_{pp}(t) + \frac{0.0017q^{-11} - 0.0017q^{-12}}{1 - 3.6q^{-1} + 4.88q^{-2} - 2.95q^{-3} + 0.67q^{-4}} T_{hf}(t) \tag{14b}$$

5. Simulation Results

The developed ES algorithm is tested with three low-level control strategies: the proposed EPSAC-MPC and two PI-like controllers. Furthermore, the performance of a PI controller that would simply maintain a constant superheating, as commonly implemented in industrial practice, is also investigated.

The heat source and heat sink profiles of the ORC system are depicted in Figure 6. The thermal oil evaporator inlet temperature is characterized by a gradual increase of 10 °C, while the other variables slightly oscillates around the operating point.
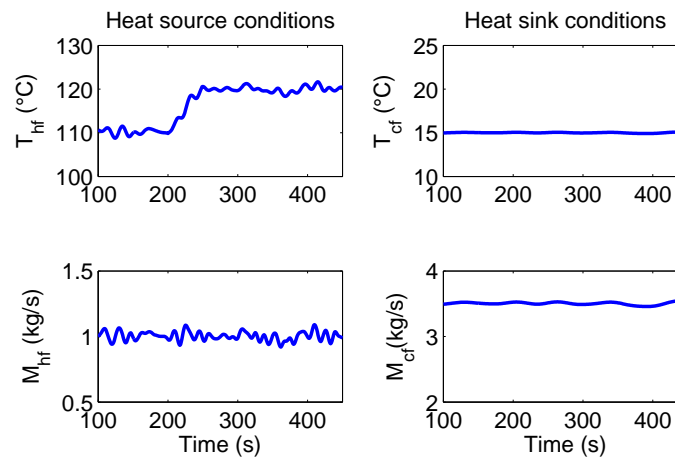
Figure 6. Heat source (**left**) and heat sink (**right**) used to test the capabilities of the proposed strategies.

5.1. Constrained EPSAC-MPC Strategy

The control objective for EPSAC-MPC consists of tracking the setpoint generated by the optimizer (Figure 3), while keeping the superheating above a desired threshold value to guarantee a safe operation. The control strategy must satisfy these conditions using only one degree of freedom (*i.e.*, pump speed N_{pp}), while satisfying actuator constraints ($N_{pp,min} = 1320$ rpm; $N_{pp,max} = 2100$ rpm; $\Delta N_{pp} = 100$ rpm) and constraints at the process output ($\Delta T_{sh,min} = 10\,°C$).

The EPSAC-MPC is designed with control horizon $N_u = 1$ and prediction horizons $N_1 = 1$, $N_2 = 15$. The ES optimizer is designed with tuning parameters: $k = 1/38$, $\omega_l = 0.02$ rad/s, $\omega_h = 0.1$ rad/s, $\gamma = 0.05$ and $\omega = 0.06$ rad/s. The results are depicted in Figure 7, where two optimal evaporating temperatures are present, one computed using the ES algorithm (dashed red line) and the other (black circles) computed from correlation in Equation (4).
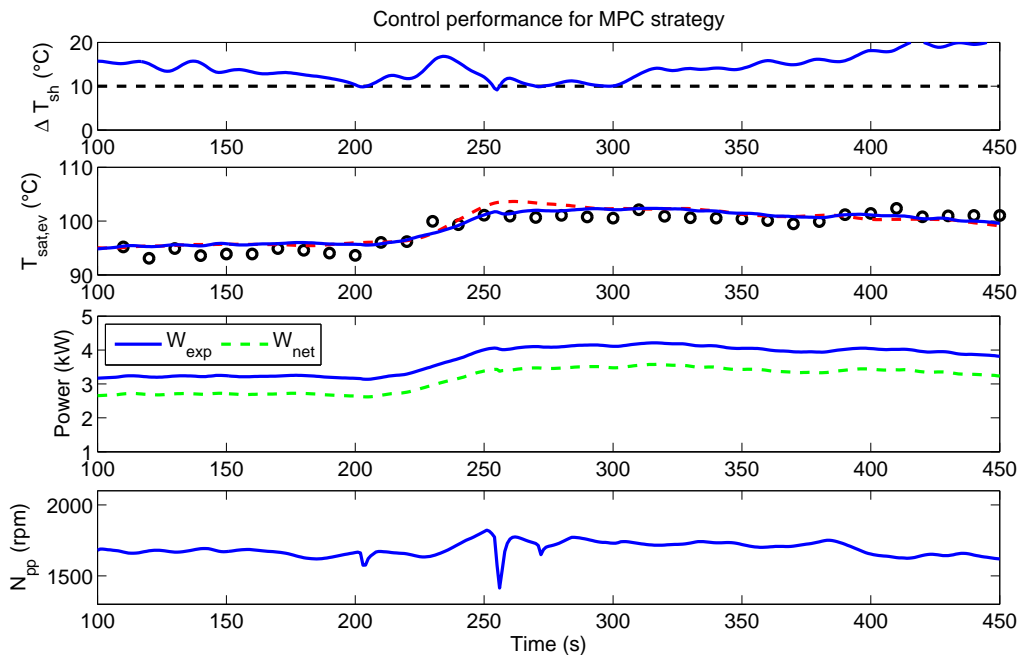

Figure 7. Control performance of MPC. The dashed red line represents the ES optimizer, while black circles represent the optimizer obtained from the dynamic model (Equation (4)).

The ES algorithm is able to adapt properly to the heat source variation, maximizing the output power. Notice that in the time range between 250 and 300 s, the controller is not following the ES setpoint. The latter is due to the active constraint in superheating, which causes the controller to take actions in the pump to bring the system to a safer regime (*i.e.*, $\Delta T_{sh} > 10\,°C$).

5.2. PI-Like Strategies

The performance of the MPC regulator is compared with two PI-like strategies.

1. Single PI strategy: a PI controller for evaporating temperature, PI_{Tsat}, is used to track the reference given by the ES optimizer.
2. Switching PI strategy: this consists of using a PI controller, PI_{Tsat}, to track the optimal evaporating temperature, unless superheating goes below the threshold value of 10 °C, in which case, a second PI controller for superheating, PI_{DT}, with reference at $\Delta T_{sh} = 10\,°C$, is enabled, thus bringing the system back into a safer regime.

The results for the single PI strategy are depicted in Figure 8. The ES optimizer (dashed red line) adapts the reference to the local PI controller, PI_{Tsat}, towards the optimal evaporating temperature, $T_{sat,opt}$, in order to maximize the output power. As the superheating is not controlled, the ORC unit is brought to hazardous working conditions characterized by a two-phase state (*i.e.*, gas and liquid phase) at the expander inlet as observed at time 250–300 s and 350–400 s.
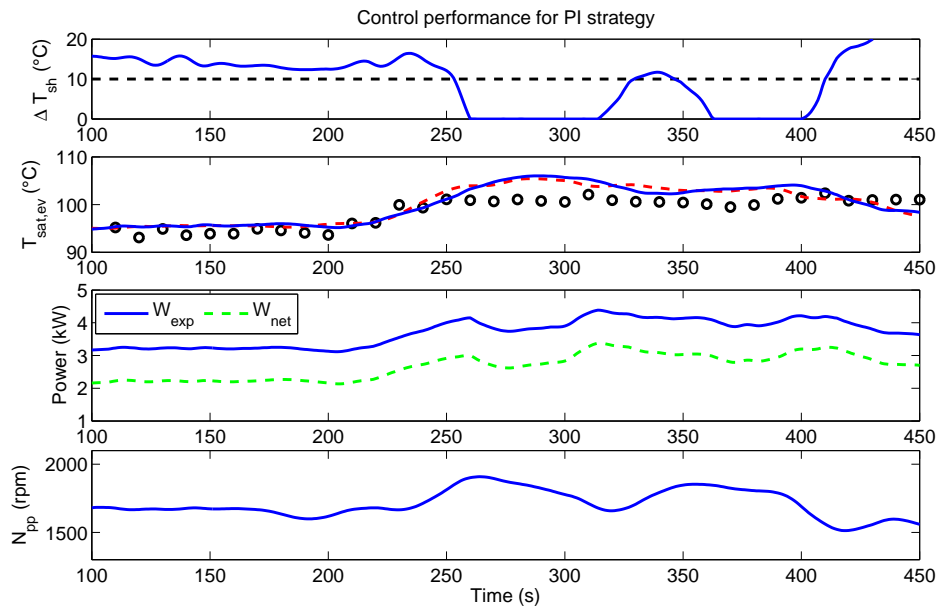

Figure 8. Control performance for a PI strategy. The dashed red line represents the ES optimizer, while black circles represent the optimizer obtained from the dynamic model (Equation (4)).

The performance of the switching PI-like strategy is reported in Figure 9. The PI_{Tsat} controller tracks the reference generated by the ES optimizer, unless the superheating value goes below a threshold value, in which case the PI_{DT} controller with reference at $\Delta T_{sh} = 10\,°C$ is enabled. The latter takes the system back to a safe operating condition, avoiding the two-phase state at the expander inlet.
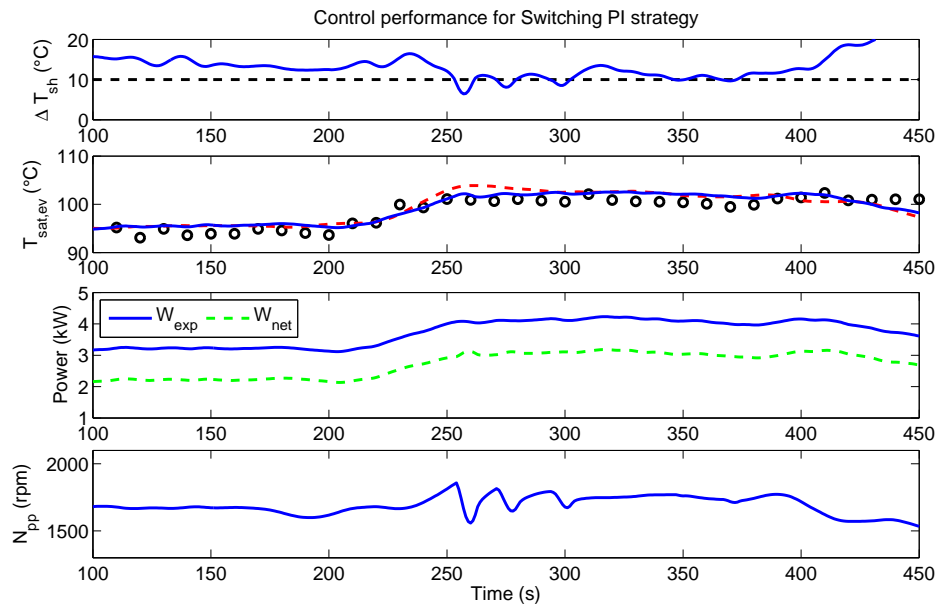
Figure 9. Control performance for a switching PI strategy. The dashed red line represents the ES optimizer, while black circles represent the optimizer obtained from the dynamic model (Equation (4)).

Despite the adoption of two controllers, super-heating values below $10\,^{\circ}$C are registered during operation from time 250–300 s. Furthermore, more aggressive control actions are imposed on the pump rotational speed compared to the MPC methodology.

In order to assess the capabilities of the proposed control strategies to maximize the ORC unit performance, the net energy generation is computed by integrating the net output power over the simulation time. As the single PI strategy is not able to ensure safety conditions, it is discarded from this comparison. Taking the switching PI as a reference (100%), the EPSAC-MPC strategy allows increasing the net energy production by 15%. This is due to a better handling of the constraints, thus operating the system closer to the constraint for superheating while requiring a lower control effort (*i.e.*, less power consumption in the pump).

5.3. Superheating Control Strategy

Many contributions available in the literature and most of approaches followed in industrial practice suggest the use of a controller that would simply maintain a constant superheating. It is therefore interesting to investigate its performance and to compare it to the approach proposed in this paper.

The PI controller in charge of regulating superheating is tuned, making a trade-off between diminishing the output variability (*i.e.*, minimizing the tracking error) and the required control effort. The reference for the controller is set at $\Delta T_{sh} = 14\,^{\circ}$C, in order to get an extra safety margin, thus avoiding superheating going below the desired minimum limit (*i.e.*, $\Delta T_{sh} = 10\,^{\circ}$C).

The PI controller is able to regulate the superheating level around the setpoint, respecting almost at all times the superheating safety limit of $10\,^{\circ}$C (Figure 10). In terms of power production, it sometimes outperforms the ES with a low-level controller as observed from time 350–450 s, where, due to the active constraint, the controllers allow a larger tracking error in order to bring the system to a safer regime.

Although the controller for superheating is performing well, it requires more aggressive control actions, leading to a higher pump power consumption. The net energy output is thus reduced and lower compared to the proposed strategy using ES and a low-level controller. Computing the net energy produced, the PI superheating controller generates (3%) more compared to the switching PI strategy, but (12%) less if compared to the ES-MPC approach.
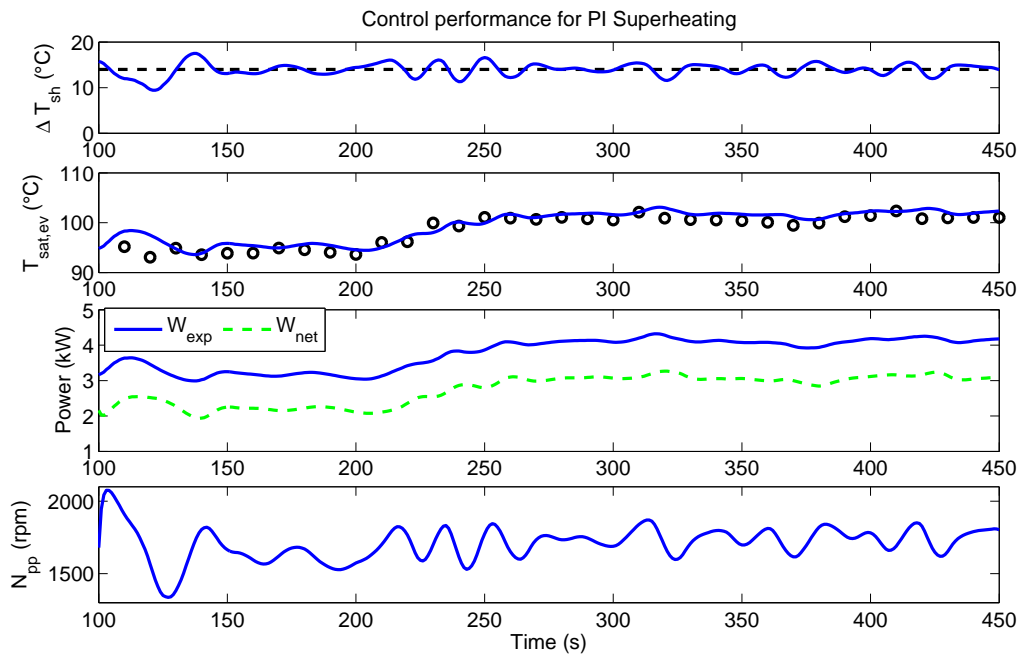
Figure 10. Control performance for the superheating PI strategy, with the reference at $\Delta T_{sh} = 14\,^{\circ}\mathrm{C}$.

6. Guidelines for ES Tuning and the Stability Test

The perturbation-based extremum seeking algorithm includes five parameters that should be tuned: the cut frequencies of the low ω_l and high ω_h pass filters, the integrator gain k, the amplitude γ and frequency ω of the dither signal. This section is an attempt to provide guidelines for the ES parametrization.

Selecting the dither frequency ω is a trade-off between the speed of convergence and precision. The dither signal should vary slowly enough for the plant to settle, thus preventing the plant dynamics from interfering with the peak seeking scheme [32]. On the other hand, increasing the dither frequency allows the integrator gain to be increased proportionally, while retaining the same domain of attraction [36]. As a rule of thumb, the dither frequency should be slower than the open-loop dynamics of the plant to obtain a useful signal to noise ratio (SNR) at the input of the ES scheme. It is worth mentioning that although the exact bandwidth of the plant is unknown, the low-order model used for MPC can be used to determine a suitable value for ω.

The value of the integrator gain k is a trade-off between the speed of convergence, precision and stability. A higher gain results in faster convergence, but the influence of any noise present in the output of the low pass filter becomes more dominant. Furthermore, there is an upper limit on the integrator gain with respect to the stability of the adaptation loop. Increasing the integrator beyond this value will render the adaptation unstable [37].

The amplitude of the dither signal is a trade-off between accuracy and precision. A large γ results in a larger offset with respect to the optimal point [36]. On the other hand, a smaller γ leads to a reduction in precision, as the decrease in the amplitude of the modulated gradient brings a deterioration of the SNR at the input of the ES scheme.

In order to investigate the stability and robustness of the presented adaptive control strategy, a second test is performed including measurement noise, as well as large variations in the heat source mass flow rate $\dot{m}_{hf}$. The heat source and heat sink profiles used for the test are depicted in Figure 11.
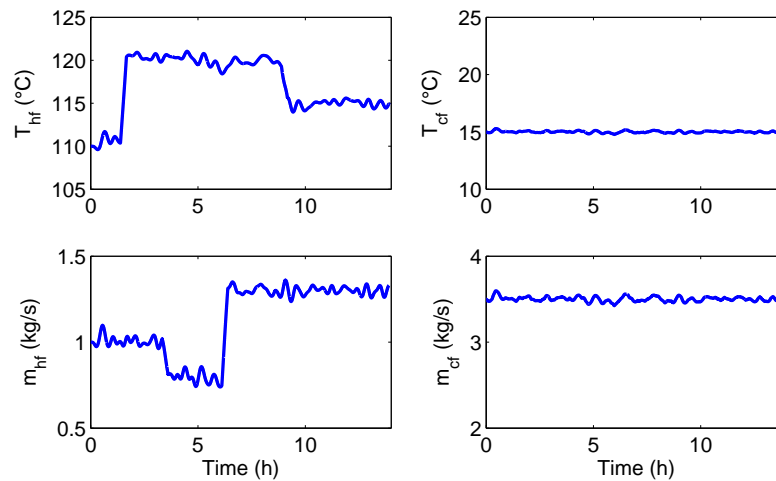
Figure 11. Temperature and mass flow rate variations in the heat source (**left**) and heat sink (**right**) employed to test the capabilities of the proposed adaptive constrained strategy.

In Figure 12, the performance of the proposed constrained adaptive strategy is tested when using a dither signal amplitude of $\gamma = 0.02$. The algorithm faces some problems to quickly converge to the optimal evaporating temperature, represented by the dashed black line obtained from Equation (4). This is due to the low SNR obtained using such a low amplitude of the dither signal. The system, although stable, is not performing optimally as concluded by observing the 'high' level of superheating obtained and the power generated.

A new experiment is performed using the same external conditions, but increasing the dither signal amplitude by two, *i.e.*, $\gamma = 0.04$. By increasing the value for γ, the SNR is increased, thus making it possible for the algorithm to quickly converge close to the optimal value, as reported in Figure 13. Attention has to be paid to avoid increasing this value unnecessarily, as a large γ could result in a larger offset with respect to the optimal point [36].
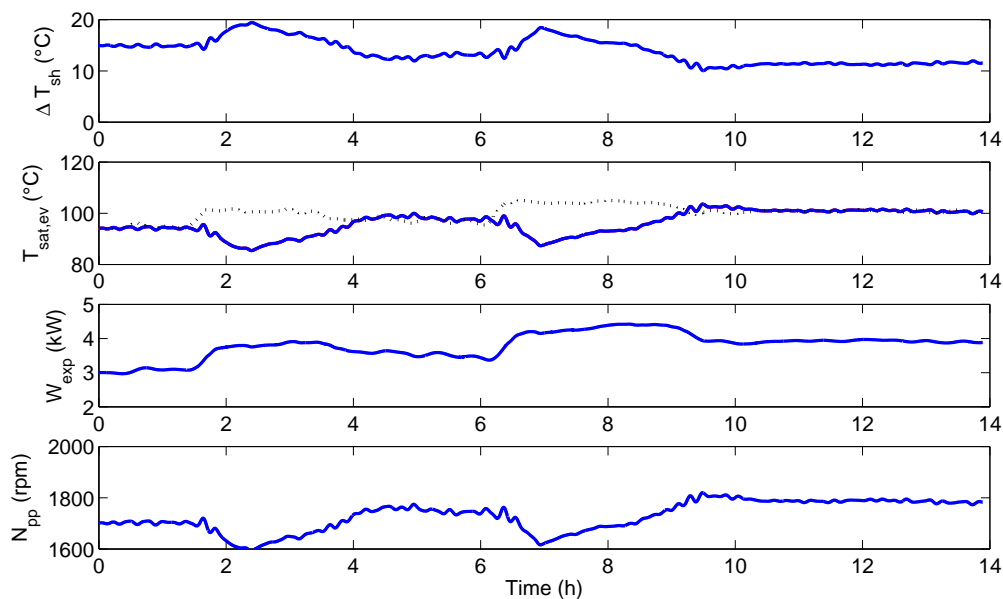

Figure 12. Control performance of the proposed adaptive constrained strategy for large heat source variations and measurement noise, using $\gamma = 0.02$.
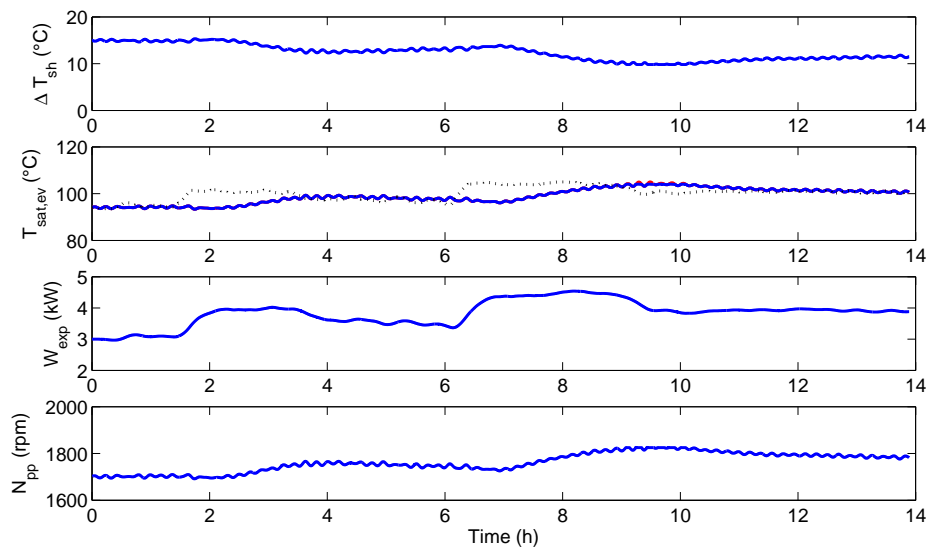
Figure 13. Control performance of the proposed adaptive constrained strategy for large heat source variations and measurement noise, using $\gamma = 0.04$.

7. Conclusions

In this contribution, a two-layer control structure to achieve constrained optimal operation of an organic Rankine cycle unit for waste heat recovery applications is proposed. It is based on an extremum seeking algorithm in the high layer and a constrained model predictive control in the low layer. The convergence accuracy of the proposed optimizer is investigated by comparing its results to the optimal evaporating temperature obtained using the model of the system. Its stability and robustness is assessed for the case of measurement noise, providing some guidelines to avoid instability or an inconsistent estimation. Furthermore, safety and energy production are investigated when comparing the performance obtained for MPC and two different low-level PI-like control schemes; and for the case of a PI controller to maintain a constant superheating.

In light of the simulation study performed, the following conclusions are drawn:

- A validated dynamic model of an $11\,kW_{el}$ sub-critical organic Rankine cycle unit for waste heat recovery application is used to illustrate the existence of an optimal evaporating temperature, which maximizes energy production for some given heat source conditions.
- The extremum seeking strategy allows determining the optimal operating conditions of the ORC system without the need for a model, thus dealing with possible modeling errors that could cause a bias in the estimation. Some guidelines to properly tune the ES algorithm are presented, where it has been shown that a low signal to noise ratio due to measurement noise can influence the convergence of the adaptive optimizer and how the amplitude of the dither signal can be used to recover the system performance.
- The MPC control strategy outperforms in terms of energy generation the PI-like strategies. It is shown that a single PI regulating the evaporation temperature cannot guarantee safety conditions; therefore, a switching PI is proposed, resulting in a safer operation compared to a single PI, but being less effective compared to model predictive control, since it violates the safety limit for superheating.
- In terms of energy production, the proposed adaptive constrained strategy provides a more efficient operation, as it requires less control effort and operates closer to the boundary conditions, thus offering a higher *net* energy production compared to PI strategies. When compared to traditional control strategies aiming at maintaining a constant superheating, the gain is about 12% for the proposed test case.

Future work will include the development of a multivariable control strategy by making use of the expander speed, as an additional manipulated variable.

Author Contributions: Andres Hernandez and Sylvain Quoilin defined the general framework and the potential benefits of extremum seeking in waste heat recovery systems. Andres Hernandez designed and implemented the extremum seeking algorithm and the control strategies and performed the system identification. Adriano Desideri developed the dynamic model and contributed with the analysis of the thermodynamic optimal conditions of the cycle. Clara Ionescu, Robin De Keyser, Vincent Lemort and Sylvain Quoilin contributed to the analysis of the stated problem, collaborated with advice in the control design and with the analysis of the results. All authors took part in the discussion and preparation of the manuscript.

Conflicts of Interest: The authors declare no conflict of interest.

Abbreviations

ORC	organic Rankine cycle	
WHR	waste heat recovery	
MPC	model predictive control	
EPSAC	extended prediction self-adaptive control	
PI	proportional-integral control	
ES	extremum seeking	
Δ	difference	
s	Laplace complex variable	
$\dot{m}$	mass flow	(kg/s)
$\dot{W}$	power	(W)
N	rotational speed	(rpm)
p	pressure	(Pa)
T	temperature	(°C)

Subscript

el	electrical
ev	evaporator
exp	expander
pp	pump
hf	hot fluid
cf	cold fluid
sh	super-heated

Greek letter

η	efficiency
γ	amplitude dither signal
ξ	gradient direction
k	integrator gain
ω	frequency dither signal
α	time constant MPC

References

1. Berntsson, T.; and Åsblad, C. *Industrial Excess Heat Recovery: Technologies & Applications*; Technical Report; Industrial Energy-Related Technologies and Systems (IETS): Göteborg, Sweden, 2015.
2. Verneau, A. Waste heat recovery by organic fluid rankine cycle. In Proceedings of the First Industrial Energy Technology Conference, Houston, TX, USA, 22–25 April 1979; pp. 940–952.

3. David, G.; Michel, F.; Sanchez, L. Waste heat recovery projects using organic Rankine cycle technology examples of biogas engines and steel mills applications. In Proceedings of the World Engineers Convention, Geneva, Switzerland, 4–9 September 2011.

4. Quoilin, S.; Van Den Broek, M.; Declaye, S.; Dewallef, P.; Lemort, V. Techno-economic survey of organic rankine cycle (ORC) systems. *Renew. Sustain. Energy Rev.* **2013**, *22*, 168–186.

5. Sprouse, C.; Depcik, C. Review of organic Rankine cycles for internal combustion engine exhaust waste heat recovery. *Appl. Therm. Eng.* **2013**, *51*, 711–722.

6. Maraver, D.; Royo, J.; Lemort, V.; Quoilin, S. Systematic optimization of subcritical and transcritical organic Rankine cycles (ORCs) constrained by technical parameters in multiple applications. *Appl. Energy* **2014**, *117*, 11–29.

7. Yang, K.; Zhang, H.; Song, S.; Yang, F.; Liu, H.; Zhao, G.; Zhang, J.; Yao, B. Effects of Degree of Superheat on the Running Performance of an Organic Rankine Cycle (ORC) Waste Heat Recovery System for Diesel Engines under Various Operating Conditions. *Energies* **2014**, *7*, 2123–2145.

8. Wei, D.; Lu, X.; Lu, Z.; Gu, J. Performance analysis and optimization of Organic Rankine Cycle (ORC) for waste heat recovery. *J. Energy Convers. Manag.* **2007**, *Vol. 48*, 1113–1119.

9. Hou, G.; Sun, R.; Hu, G.; Zhang, J. Supervisory Predictive Control for Evaporator in Organic Rankine Cycle (ORC) System for Waste Heat Recovery. In Proceedings of the International Conference on Advanced Mechatronics Systems, Zhengzhou, China, 11–13 August 2011; pp. 306–311.

10. Lemort, V.; Zoughaib, A.; Quoilin, S. Comparison of control strategies for waste heat recovery Organic Rankine Cycle systems. In Proceedings of the Sustainable Thermal Energy Management in the Process Industries International Conference (SusTEM2011), Newcastle upon Tyne, UK, 25–26 October 2011.

11. Peralez, J.; Tona, P.; Lepreux, O.; Sciarretta, A.; Voise, L.; Dufour, P.; Nadri, M. Improving the control performance of an organic rankine cycle system for waste heat recovery from a heavy-duty diesel engine using a model-based approach. In Proceedings of the IEEE Conference on Decision and Control, Florence, Italy, 10–13 December 2013.

12. Grelet, V.; Dufour, P.; Nadri, M.; Lemort, V.; Reichel, T. Explicit multi-model predictive control of a waste heat Rankine based system for heavy duty trucks. In Proceedings of the IEEE Conference on Decision and Control, Osaka, Japan, 15–18 December 2015.

13. Zhang, J.; Zhou, Y.; Li, Y.; Hou, G.; Fang, F. Generalized predictive control applied in waste heat recovery power plants. *Appl. Energy* **2013**, *102*, 320–326.

14. Hernandez, A.; Desideri, A.; Ionescu, C.; Quoilin, S.; Lemort, V.; De Keyser, R. Increasing the efficiency of Organic Rankine Cycle Technology by means of Multivariable Predictive Control. In Proceedings of the 19th World Congres World Congress of the International Federation of Automatic Control (IFAC 2014), Cape Town, South Africa, 24–29 August 2014.

15. Quoilin, S.; Aumann, R.; Grill, A.; Schuster, A.; Lemort, V. Dynamic modeling and optimal control strategy for waste heat recovery Organic Rankine Cycles. *Appl. Energy* **2011**, *88*, 2183–2190.

16. Hernandez, A.; Desideri, A.; Ionescu, C.; Quoilin, S.; Lemort, V.; De Keyser, R. Experimental study of Predictive control strategies for optimal operation of Organic Rankine Cycle systems. In Proceedings of the European Control Conference (ECC15), Linz, Austria, 15–17 July 2015.

17. Feru, E.; Willems, F.; de Jager, B.; Steinbuch, M. Modeling and Control of a Parallel Waste Heat Recovery System for Euro-VI Heavy-Duty Diesel Engines. *Energies* **2014**, *7*, 6571–6592.

18. Peralez, J.; Tona, P.; Nadri, M.; Dufour, P.; Sciarretta, A. Optimal control for an organic rankine cycle on board a diesel-electric rail car. *J. Process Control* **2015**, *33*, 1–13.

19. Ariyur, K.; Krstic, M. *Real-Time Optimization by Extremum-Seeking Control*; John Wiley & Sons: Hoboken, NJ, USA, 2003.

20. Koeln, J.P.; Alleyne, A.G. Optimal subcooling in vapor compression systems via extremum seeking control: Theory and experiments. *Int. J. Refrig.* **2014**, *43*, 14–25.

21. Singh, R.; Kearney, M.P.; Manzie, C. Extremum-seeking control of a supercritical carbon-dioxide closed Brayton cycle in a direct-heated solar thermal power plant. *Energy* **2013**, *60*, 380–387.

22. Weiss, W.; Burns, D.; Guay, M. Realtime Optimization of MPC Setpoints using Time-Varying Extremum Seeking Control for Vapor Compression Machines. In Proceedings of the 15th International Refrigeration and Air Conditioning Conference at Purdue, West Lafayette, IN, USA, 14–17 July 2014; pp. 1–10.

23. De Hann, D.; Guay, M. Extremum-Seeking control of state-constrained nonlinear systems. *Automatica* **2005**, *41*, 1567–1574.

24. Maciejowski, J. *Predictive Control: With Constraints*; Prentice-Hall/Pearson Education Limited: Harlow, UK, 2002.

25. Desideri, A.; Dechesne, B.; Wronski, J.; Van Den Broek, M.; Gusev, S.; Lemort, V.; Quoilin, S. Comparison of Moving Boundary and Finite-Volume heat exchanger models in the modelica language. *Energies* **2016**, in press.

26. Desideri, A.; Gusev, S.; van den Broek, M.; Lemort, V.; Quoilin, S. Experimental comparison of organic fluids for low temperature ORC (organic Rankine cycle) systems for waste heat recovery applications. *Energy* **2016**, *97*, 460–469.

27. Quoilin, S.; Desideri, A.; Wronski, J.; Bell, I.; Lemort, V. ThermoCycle: A Modelica library for the simulation of thermodynamic systems. In Proceedings of the 10th International Modelica Conference, Lund, Sweden, 10–12 March 2014.

28. Bendapudi, S.; Braun, J.; Groll, E. A comparison of moving-boundary and finite-volume formulations for transients in centrifugal chillers. *Int. J. Refrig.* **2008**, *31*, 1437–1452.

29. Desideri, A.; Van Den Broek, M.; Gusev, S.; Lemort, V.; Quoilin, S. Experimental campaign and modeling of a low-capacity waste heat recovery system based on a single screw expander. In Proceedings of the 22nd International Compressor Engineering Conference at Purdue, West Lafayette, IN, USA, 14–17 July 2014; pp. 1–10.

30. Bell, I.; Wronski, J.; Quoilin, S.; Lemort, V. Pure and Pseudo-pure Fluid Thermophysical Property Evaluation and the Open-Source Thermophysical Property Library CoolProp. *Ind. Eng. Chem. Res.* **2014**, *53*, 2498–2508.

31. Zhang, C.; Ordonez, R. *Extremum-Seeking Control and Applications. A Numerical Optimization-Based Approach*; Advances in Industrial Control; Springer-Verlag: London, UK, 2012.

32. Krstic, M. Performance improvement and limitations in extremum seeking control. *Syst. Control Lett.* **2000**, *9*, 313–326.

33. De Keyser, R. *Model Based Predictive Control for Linear Systems*; Invited Chapter in UNESCO Encyclopedia of Life Support Systems (EoLSS); EoLSS publishers: Oxford, UK, 2003.

34. Camacho, E.F.; Bordons, C. *Model Predictive Control*, 2nd ed.; Springer-Verlag: London, UK, 2004; Volume 405.

35. Ljung, L. *System Identification: Theory for the User*; Prentice-Hall: Englewood Cliffs, NJ, USA, 2007.

36. Tan, Y.; Nesic, D.; Mareels, I. On non-local stability properties of extremum seeking control. *Automatica* **2006**, *44*, 889–903.

37. Moase, W.; Manzie, C.; Brear, M. Newton-like extremum-seeking for the control of thermoacustic instability. *IEEE Trans. Autom. Control* **2010**, *55*, 2094–2105.